Nano Energy (2015) 11, 419–427

Available online at www.sciencedirect.com

ScienceDirect

journal homepage: www.elsevier.com/locate/nanoenergy

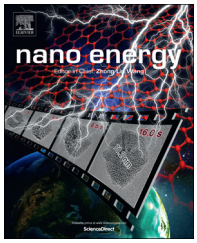

RAPID COMMUNICATION

Carbon quantum dots/hydrogenated TiO_2 nanobelt heterostructures and their broad spectrum photocatalytic properties under UV, visible, and near-infrared irradiation

Jian Tian[a,b,1], Yanhua Leng[b,1], Zhenhuan Zhao[b], Yang Xia[c], Yuanhua Sang[b], Pin Hao[b], Jie Zhan[b], Meicheng Li[d,**], Hong Liu[a,b,*]

[a]Beijing Institute of Nanoenergy and Nanosystems, Chinese Academy of Science, Beijing 100083, China
[b]State Key Laboratory of Crystal Materials, Shandong University, Jinan 250100, China
[c]College of Materials Science and Engineering, Zhejiang University of Technology, Hangzhou 310014, China
[d]School of Renewable Energy, North China Electric Power University, Beijing 102206, China

Received 19 September 2014; received in revised form 26 October 2014; accepted 26 October 2014
Available online 4 November 2014

KEYWORDS
Photocatalytic;
Near-infrared;
Hydrogenation;
TiO_2 nanobelt;
Carbon quantum dots

Abstract
To make the best and highest use of solar light is the main direction and object of photocatalysis and water-splitting. Although UV and visible active photocatalysts have been extensively investigated, the use of near-infrared (NIR) wave band of solar light remains a nearly blank area. Here we report the UV-visible-NIR broad spectrum active photocatalytic property of CQDs/hydrogenated TiO_2 (H-TiO_2) nanobelt heterostructures. The improved UV and visible photocatalytic property can be attributed to improved optical absorption, charge carrier trapping, and hindering of the photogenerated electron-hole recombination of oxygen vacancies and Ti^{3+} ions in TiO_2 nanobelts created by hydrogenation. The NIR photocatalytic activity is from photo-induced electron transfer, electron reservoir, and up-converted PL properties of CQDs, which can absorb NIR light and convert into visible light and transfer to visible photocatalytic active H-TiO_2 nanobelts. This work offers a simple strategy for the fabrication of a wide spectrum of active heterostructured photocatalysts by assembling CQDs on the surface of UV-visible photocatalysts, which opens a door for photodegradation, photocatalytic water splitting, and enhanced solar cells using sunlight as light source.

*Corresponding author at: Beijing Institute of Nanoenergy and Nanosystems, Chinese Academy of Science, Beijing 100083, China.
**Corresponding author.
E-mail addresses: mcli@ncepu.edu.cn (M. Li), hongliu@sdu.edu.cn (H. Liu).
[1]These authors contributed equally.

http://dx.doi.org/10.1016/j.nanoen.2014.10.025
2211-2855/

Introduction

The present energy crisis and environmental contamination makes it necessary to explore renewable and clean energy sources [1–3]. As one of the most promising renewable and clean energy sources in the world, solar energy offers a free, clean, non-polluting, inexhaustible resource [4–6]. The search for semiconductor photocatalysts that can harvest the wide spectrum of solar light, from ultraviolet (UV) to near-infrared (NIR) to achieve efficient solar energy conversion is the main driving force for the development of new and efficient photocatalysts [7].

Titanium dioxide (TiO_2), one of the most promising photocatalysts, has attracted considerable attention and been widely applied in photovoltaics, photoelectrochemical cells, photocatalysts and gas sensing [8–12]. Unfortunately, the wide band gap of TiO_2 (3.2 eV) has limited its widespread application because it is activated solely by UV light, which makes up only 5% of the total incoming solar radiation [13–16]. Visible light accounts for about 42–45% of sunlight, so numerous efforts to develop photocatalysts that are effective in this portion of the spectrum, including N-doped TiO_2, hydrogenated TiO_2 (H-TiO_2), and bismuth-based photocatalysts [17–19]. Nevertheless, NIR light, accounting for more than 50% of the solar spectrum, remains underutilized [4]. Only a few NIR photocatalysts have been investigated, such as up-conversion materials, Bi_2WO_6, $Cu_2(OH)PO_4$, and carbon quantum dots (CQDs) [20–23]. At present, most photocatalysts are driven by artificial sunlight, but their real target should be the harvesting of all solar light. Therefore, a broad spectrum (UV–vis–NIR) light active photocatalyst should be a high priority for practical photo-electric conversion materials.

Hydrogenation, a simple method for extending the absorption spectrum of TiO_2-based materials into the visible light region without suppressing their UV light photocatalysis property, allows expansion of their applications into areas beyond photocatalysis, lithium ion batteries, and solar cells [24–26]. Hydrogenation of the surface of anatase TiO_2 to introduce surface disorder and oxygen vacancies, leads to the creation of Ti^{3+} centers or unpaired electrons, and subsequently forms donor levels in the electronic structure of TiO_2 [27,28]. Oxygen vacancies are believed to suppress the recombination of photo-generated electrons and holes, improving the photocatalytic activity of TiO_2 [29].

Carbon quantum dots, as a novel class of recently discovered carbon nanomaterials, have attracted much attention because of their fascinating physical and chemical properties [30]. These include high aqueous solubility, high biocompatibility, low toxicity, photo-induced electron transfer, redox properties, and luminescence [31]. Notably, they possess both up- and down-converted photoluminescence (PL), and electron-accepting and -transport properties, which make CQDs-based NIR light sensitive hybrid photocatalysts become promising agents for harvesting NIR light [32,33]. Although CQDs can be assembled on the surface of some UV or visible photocatalytic-active nanoparticles to yield UV–NIR and vis–NIR light active photocatalysts, their low photocatalytic activity and non-recyclability restrict their application. Discovering high efficiency and practical CQDs-based broad spectrum (UV–vis–NIR) light active photocatalysts remains a challenge.

Therefore, in order to improve the use of the full spectrum of solar energy, a novel heterostructure, which consist of NIR light induced CQDs' up-conversion phosphor, and UV and visible lights driven H-TiO_2 nanobelts photocatalysts, was prepared by the synthesis of TiO_2 nanobelts followed by subsequent hydrogenation and bath reflux CQDs loading strategy (Figure 1a). The photocatalytic activities of the as-prepared heterostructures were evaluated by the degradation of methylene orange (MO) in aqueous solution upon UV, visible, and NIR light irradiation. Importantly, the CQDs/H-TiO_2 heterostructures showed significantly improved photocatalytic activities under UV and visible light irradiation in comparison with H-TiO_2 nanobelts and TiO_2 nanobelts, and also exhibited NIR active photocatalytic activity. CQDs with NIR up-conversion activity might serve as an intermedium, which transfers energy from NIR light to visible light, which is absorbed by H-TiO_2 nanobelts to generate strongly oxidative holes and reductive electrons, improving the photocatalytic property. These results contribute to the structural design and functionality improvement of this new type of broad spectrum catalytic material.

Experimental section

Materials

The chemicals used in this work were of analytical reagent grade. Titania P25 (anatase 80%, rutile 20%, Degussa Co. Ltd., Germany), sodium hydroxide (NaOH), hydrochloric acid (HCl), sulfuric acid (H_2SO_4) and glucose were purchased from Sinopharm and used without further treatment.

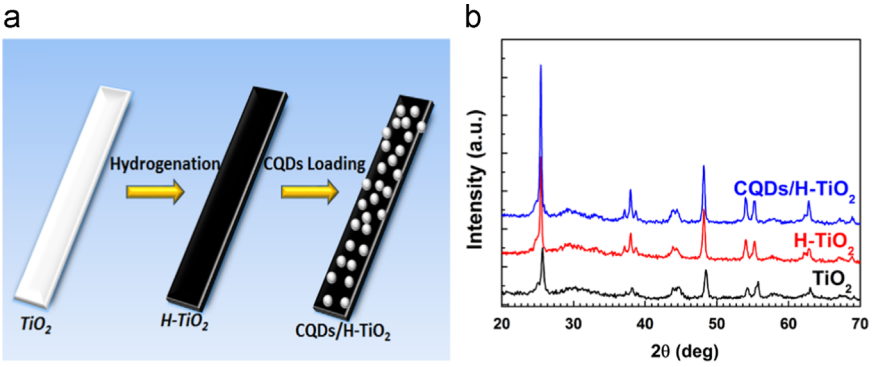

Figure 1 (a) Schematic illustration of the fabrication process of CQDs/H-TiO_2 heterostructure and (b) XRD patterns of TiO_2 nanobelts, H-TiO_2 nanobelts, and CQDs/H-TiO_2 heterostructures.

Synthesis

Preparation of hydrogenated TiO_2 (H-TiO_2) nanobelts: TiO_2 nanobelts were synthesized by a hydrothermal procedure. Typically, P25 powder (0.1 g) was mixed with an aqueous solution of NaOH (20 mL, 10 mol/L), followed by a hydrothermal treatment at 180 °C in a 25 mL Teflon-lined autoclave for 48 h. The treated powder was washed thoroughly with deionized water followed by filtration and drying processes. The obtained sodium titanate nanobelts were then immersed in an aqueous solution of HCl (0.1 mol/L) for 48 h and then washed thoroughly with water to produce $H_2Ti_3O_7$ nanobelts. The $H_2Ti_3O_7$ nanobelts were added into a 25 mL Teflon vessel, which was filled with an aqueous solution of H_2SO_4 (0.02 mol/L) up to 80% of the total volume and maintained at 100°C for 12 h. Finally, the products were isolated from the solution by centrifugation and sequentially washed with deionized water several times, and dried at 70 °C for 10 h. Thermal annealing of the $H_2Ti_3O_7$ nanobelts by acid corrosion at 600 °C for 2 h led to the production of TiO_2 nanobelts with roughened surfaces. The H-TiO_2 nanobelts were obtained by annealing the TiO_2 nanobelts in hydrogen atmosphere at temperature at 600 °C for 60 min. Thermal treatment was performed in tube furnace filled with hydrogen and argon gas mixtures (1:1).

Preparation of carbon quantum dots (CQDs): CQDs were synthesized by a facile one-step alkali-assisted ultrasonic treatment. In a typical experiment, 0.05 mol glucose was dissolved in 50 mL deionized water to form a clear solution. Then 50 mL NaOH solution (1 mol/L) was added to the solution of glucose, and the mixed solution was submitted to a 150 W (40 kHz) ultrasonic treatment for 2 h at room temperature. Then, the raw solution obtained from glucose/NaOH was adjusted to pH=7 with HCl. After that, the crude solution underwent dialysis treatment using a semipermeable membrane (MWCO 1000) to remove any impurities except for the CQDs sample. After filter treatment, the obtained solution was brown, implying the formation of CQDs.

Preparation of CQDs/H-TiO_2 heterostructures: To synthesize CQDs/H-TiO_2 heterostructures, 0.08 g H-TiO_2 nanobelts were added into 50 mL CQDs aqueous solution. Then the heterostructures were obtained via an oil bath reflux at 90 °C for 3 h. The obtained samples were washed with water, and then dried in an oven at 60 °C for 12 h.

Materials characterization

X-ray powder diffraction (XRD) pattern of catalysts were recorded on a Bruke D8 Advance powder X-ray diffractometer with Cu Kα (λ=0.15406 nm). HITACHI S-4800 field emission scanning electron microscope (FE-SEM) was used to characterize the morphologies and size of the synthesized samples. The chemical composition was investigated via energy-dispersive X-ray spectroscopy (EDS). High resolution transmission electron microscopy (HRTEM) images were carried out with a JOEL JEM 2100 microscope. X-ray photoelectron spectroscopy (XPS) was performed using an ESCALAB 250. Fourier transform infrared (FTIR) spectra were collected on a Nicolet Avatar 370 infrared spectrometer in the range 400–4000 cm^{-1} using pressed KBr discs. The KBr disks were formed by mixing 10 mg of each sample with 1000 mg of KBr in an agate mortar. From this stock, 200 mg were then pressed into pellets of 13 mm diameter. UV–vis–NIR diffuse reflectance spectra (DRS) of the samples were recorded on a UV–vis-NIR spectrophotometer (Cary 5000, Varian) with an integrating sphere attachment within the range of 200–2000 nm and with $BaSO_4$ as the reflectance standard. The photoluminescence (PL) spectra were carried out on a Horiba JobinYvon (FluoroMax 4) Luminescence Spectrometer. The specific surface area was calculated using the Brunauer–Emmett–Teller (BET) method using a Micromeritics, ASAP2020 instrument.

Photocatalytic activity test: The photocatalytic activity of the CQDs/H-TiO_2 heterostructures was investigated by the photodegradation of methyl orange (MO, 20 mg/L) and photocatalytic hydrogen evolution. In a typical photodegradation experiment, 20 mL aqueous suspension of MO and 20 mg of photocatalyst powder were placed in a 50 mL beaker. Prior to irradiation, the suspensions were magnetically stirred in the dark for 30 min to establish adsorption-desorption equilibrium between the dye and the surface of the catalyst under normal atmospheric conditions. A 350 W mercury lamp with a maximum emission at 356 nm was used as the UV source for photocatalysis. A 300 W Xe arc lamp was used as the visible light source with filter glasses to filter UV light for visible light photocatalysis. A 250 W infrared lamp used as the NIR light source where the λ<760 nm were filtered out during NIR light photocatalysis. At given irradiation time intervals, aliquots of the mixed solution were collected and centrifuged to remove the catalyst particulates for analysis. The residual MO concentration was detected using a UV-vis spectrophotometer (Hitachi UV-3100). In a typical photocatalytic hydrogen evolution experiment, all samples were loaded with 1 wt% platinum by a photo-deposition process before photocatalytic production of H_2. Briefly, samples and chloroplatinic acid ($H_2PtCl_6 \cdot 6H_2O$, c=10 g/L) were suspended in 20:80 v/v mixture of ethanol: water, and were irradiated with a Mercury lamp (300 W) for 30 min. The catalyst (0.05 g) was suspended in 100 mL aqueous solution containing methanol (20% v/v). The reaction temperature was maintained at 5 °C. A 300 W Xe arc lamp (CEL-HXF300, Beijing Aulight Co. Ltd.) was used as the light source. The amount of H_2 evolved was determined with a gas chromatograph (Techcomp GC7900) equipped with thermal conductivity detector (TCD).

Results and discussion

Figure 1b shows the XRD pattern of TiO_2 nanobelts, H-TiO_2 nanobelts, and CQDs/H-TiO_2 heterostructures. Strong XRD diffraction peaks at 2θ=25.28°, 37.80°, 48.05°, 53.89°, 55.06°, and 62.69° in curve black and red indicate that both TiO_2 nanobelts and H-TiO_2 nanobelts displayed highly crystalline anatase phases (JCPDS 21-1272) with no crystal-phase change after hydrogenation. Further, the diffraction peak intensity increases after hydrogenation and the average grain size of TiO_2 nanobelts and H-TiO_2 nanobelts is 26.8 and 22.2 nm, respectively, deduced from peak broadening of the X-ray diffraction pattern using the Scherrer equation. Chen et al. [34] observed a peak intensity decrement during the hydrogenation process, which was ascribed to the increase of defect density in the crystal structure. However,

this phenomenon does not appear in our present study. Considering the experimental process, these results may originate from the conflict between crystal growth and high density defect formations. In curve red, a slight peak at 23.82° was observed. This peak can be perfectly indexed to the (012) crystal planes of Ti_2O_3 (JCPDS 10-0063). Ti^{3+} is known to form in H-TiO_2 nanobelts. Under thermal hydrogenation, hydrogen atoms interact dramatically with lattice oxygen on the surface of TiO_2 nanobelts; the electrons of the H atoms are transferred to the Ti^{4+} of TiO_2, and Ti^{3+} defects are formed [27]. For CQDs/H-TiO_2 heterostructures (curve blue), all of the diffraction peaks can be matched well with H-TiO_2 nanobelts. No extra peaks were found, indicating that there is no second crystalline phase in the products. The characteristic peak for carbon at 26° is too weak to be observed, which is due to the low amount of carbon and its relatively low diffraction intensity in the heterostructure [35].

The morphology and structural changes of the samples was characterized by scanning electron microscopy (SEM) and transmission electron microscopy (TEM) measurements. Figure 2a shows a typical SEM image of the TiO_2 nanobelts, which are 50–200 nm in width, 20–40 nm in thickness, and have a belt structure [14,36]. After the acid etching process, surface-coarsened TiO_2 nanobelts are obtained (Figure 2b). No obvious difference of size and morphology between H-TiO_2 nanobelts and the as-synthesized ones can be observed under SEM conditions (Figure 2c). However, the color of the nanobelt powder changes from white (inset in Figure 2b) to dark-blue (inset in Figure 2c) after hydrogenation. The blue coloration of the samples is due to the formation of Ti^{3+} ions by electron trapping at the Ti^{4+} centers. The surface-coarsened H-TiO_2 nanobelts have a large specific surface area and can provide numerous nucleation sites for the growth of CQDs. Figure 2d shows a SEM image of the CQDs/H-TiO_2 heterostructures. CQDs are difficult to discern through FE-SEM due to their very small size. Figure S1 displays the energy dispersive X-ray spectroscopy (EDS) patterns of the CQDs/H-TiO_2 heterostructures. In addition to the Ti and O peaks resulting from TiO_2, the C diffraction peaks corresponding to CQDs (CQDs content: 3.0%) can be clearly observed.

Figure 3a shows the TEM image of CQDs obtained by the glucose ultrasonic method [37]. The small CQDs appear as spherical particles with a diameter of less than 5 nm and have good monodispersity, which consistent with atomic force microscopy (AFM) of CQDs (Figure S2). Figure S3 shows the particle size distribution, and their average diameter is 4.19 nm. They freely disperse in water with a transparent appearance (Figure S4a). The bright blue luminescence can be clearly observed under UV irradiation (Figure S4b, 365 nm, center) even at very dilute concentration, indicating that the CQDs possess high down-version fluorescent properties. The high resolution TEM image (HRTEM) of CQDs is shown in Figure 3b. The lattice spacing of 0.325 nm agrees well with the (002) spacing of graphite [38,39].

After assembling CQDs on the surface of H-TiO_2 nanobelts, the CQDs/H-TiO_2 heterostructures retain a one-dimensional morphology and the surface of the TiO_2 nanobelts is homogeneously covered with a layer of dense CQDs (Figure 3c and

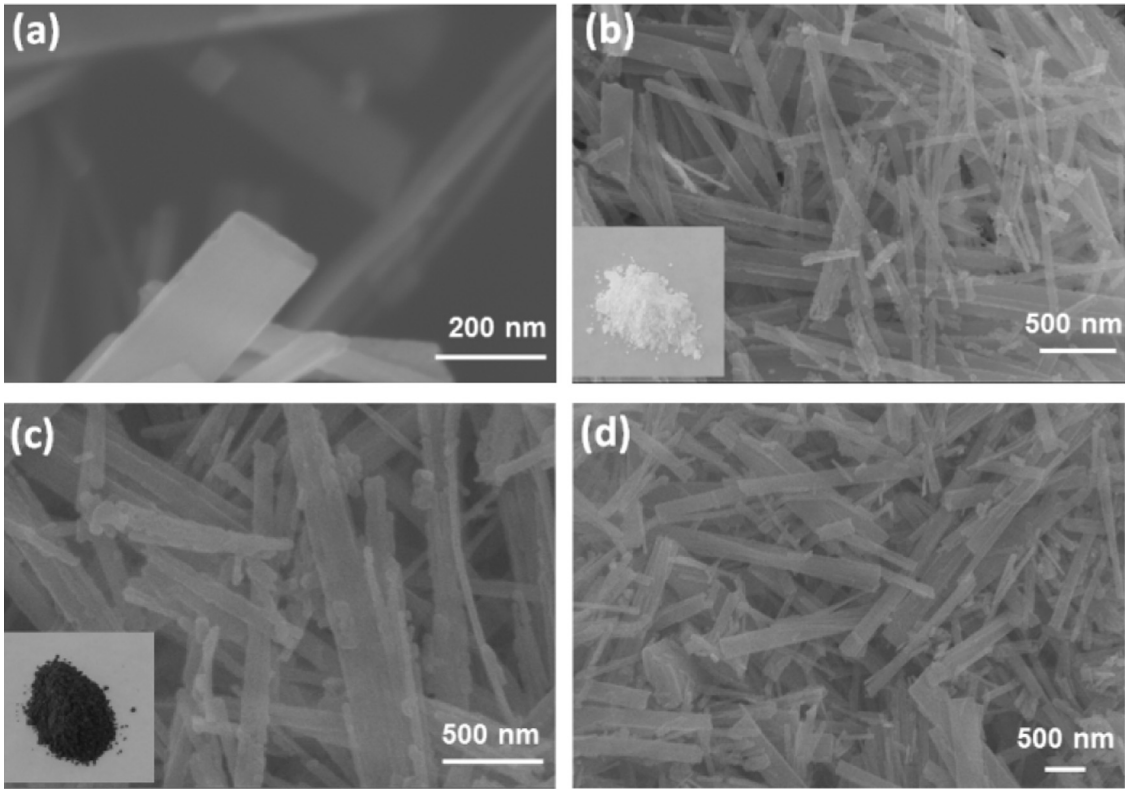

Figure 2 SEM images of (a and b) TiO_2 nanobelts. Powder of bulk TiO_2 nanobelts is shown in the bottom left inset of (b); (c) H-TiO_2 nanobelts. Powder of bulk H-TiO_2 nanobelts is shown in the bottom left inset; and (d) CQDs/H-TiO_2 heterostructures.

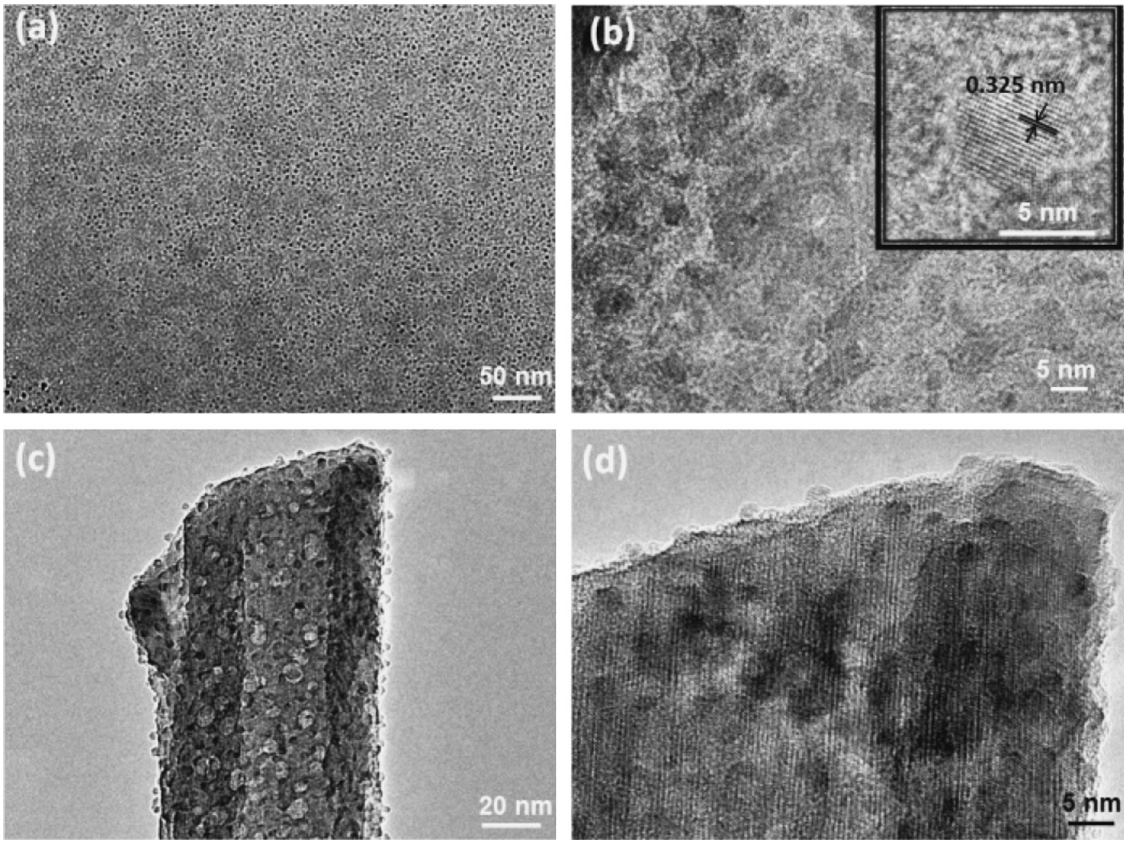

Figure 3 Low-magnification (a) and high-magnification (b) TEM images of CQDs. Insets show HRTEM images of CQDs; low-magnification (c) and high-magnification; and (d) TEM images of CQDs/H-TiO_2 heterostructures.

d). The HRTEM of CQDs/H-TiO_2 heterostructures is shown in Figure 3d and S5, revealing the interplanar spacing of 0.354 nm and 0.325 nm, which corresponds to the (101) crystal planes of anatase TiO_2 [40,41], and the (002) crystal planes of graphite, respectively. This is indicative of the formation of the heterostructure, which can benefit better charge separation and efficient electron transfer within the hybrid structure when compared with pure TiO_2 nanobelt, corroborating the enhanced photocatalytic activity.

X-ray photoelectron spectroscopy (XPS) was used to characterize the presence and chemical states of Ti in the samples. Figure S6 shows the Ti2p XPS spectra of CQDs/H-TiO_2 heterostructures. Ti^{3+} ions were found in the CQDs/H-TiO_2 heterostructures. The formation of the Ti^{3+} induces TiO_2 nanobelt's color changing from white to black [42]. The Ti^{3+}/Ti^{4+} ratio was calculated to be approximately 88.9:11.1, and the concentration of oxygen defects was calculated to be about 3%. After calculation, the 36-atom super cell of TiO_2 has one O vacancy. Oxygen vacancies on the surface or in the bulk of samples can suppress the recombination of electron-hole pairs and help to form O_{ads} by oxygen photo-adsorption thereby promoting catalytic activity [43]. Density functional theory (DFT) simulations show that oxygen vacancies in the TiO_2 crystalline structure produce visible absorption by reducing the band gap and raising the Fermi level (Figure S7). The density of states (DOS) of TiO_2 with one O vacancy also shows that the primary interband transition is still at approximately 2.17 eV (Figure S8b), similar with the DOS of pure TiO_2 (Figure S8a), however an interband transition is also possible at roughly 0.77 eV with a smaller DOS.

Figure 4a shows UV-vis-NIR absorption spectra of the TiO_2 nanobelts, H-TiO_2 nanobelts, and CQDs/H-TiO_2 heterostructures. TiO_2 nanobelts shows strong absorption in the UV region, and the absorption wavelength was approximately 380 nm (black curve), which agreed well with the bandgap of bulk anatase (E_g=3.2 eV, corresponding to λ=387 nm) [44]. The hydrogenation had little effect on the absorption of TiO_2 nanobelts in the UV region, while H-TiO_2 nanobelts exhibited a remarkable absorption in the visible light region, implying suitability for UV-visible photocatalysis (red curve in Figure 4a). The experimental absorption spectrum of H-TiO_2 nanobelts matches the theoretical spectrum well (Figure S9). It is reported that titanium oxides with lower oxidation states, such as Ti_2O_3 and TiO, usually show a strong absorption across the entire visible light range and is responsible for the bandgap narrowing in TiO_2 [45]. This strong absorption band can be attributed to the low-energy photon of trapped electrons in localized states of oxygen vacancy associated with Ti^{3+} or Ti^{2+} just below the conduction band minimum to the conduction band [46]. While CQDs/H-TiO_2 heterostructures also display obvious visible light absorption ranging from 400 to 800 nm except for strong UV absorption (blue curve in Figure 4a). Compared to the H-TiO_2 nanobelt, the large red shift from the heterostructure arises from the beneficial interaction between CQDs and H-TiO_2 nanobelts. This larger absorption

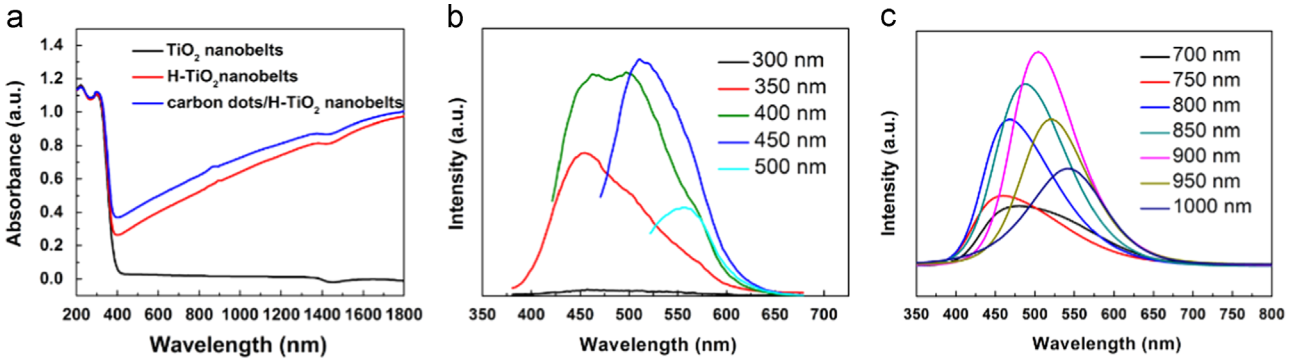

Figure 4 (a) UV-vis-NIR diffuse reflectance spectra of TiO_2 nanobelts, H-TiO_2 nanobelts, and CQDs/H-TiO_2 heterostructures; (b) down-converted and (c) up-converted photoluminescence spectra of CQDs.

would lead to the enhancement of the photocatalytic activity of CQDs/H-TiO_2 heterostructures, again indicating their usefulness for harnessing solar energy.

To further explore CQDs' optical properties, photoluminescence (PL) of the as-prepared CQDs was studied using different excitation wavelengths (Figure 4b and c). Figure 4b shows the down-converted PL spectra (300–800 nm) of CQDs within the excitation range of 300–500 nm. When the excitation wavelength changes from 320 to 480 nm, the PL peak correspondingly shifts from 430 (violet) to 560 nm (yellow). The most intense PL from the CQDs appears under a wavelength of 450 nm and has a maximum at 510 nm. Figure 4c shows the up-converted PL spectra (300–800 nm) of CQDs with excitations at 700, 750, 800, 850, 900, 950, and 1000 nm (NIR light region). We found that the emissions are located at visible light wavelengths of 300–650 nm. That is to say, CQDs have obvious up-converted PL behavior. CQDs absorb NIR light and then emit visible light (300–530 nm) as a result of up-conversion, which can in turn excite a visible light photocatalyst to form electron-hole pairs, make this visible light photocatalyst can effectively harness the broad spectrum of sunshine to strengthen the photocatalytic activities.

The photocatalytic activity of the CQDs/H-TiO_2 heterostructures was evaluated for the degradation of organic dyes (MO) in water under UV, visible and NIR light irradiation (Figure 5a–c), where C was the absorption of MO at the wavelength of 465 nm and C_0 was the absorption after the adsorption equilibrium on the samples before irradiation. For comparison, P25, TiO_2 nanobelts, and H-TiO_2 nanobelts were used as a photocatalytic references to measure under the same experimental conditions. Before the photocatalysis, blank experiments were performed under various conditions: (1) the solution including MO and photocatalysts was stirred in the dark for the adsorption equilibrium (Figure 5a–c), and (2) with UV, visible, and NIR light irradiation in the absence of the photocatalysts (Figure S10). These results highlighted that the samples by themselves exhibited no catalytic activity or absorption on MO in the dark. Furthermore, only a negligible amount of the MO was degraded after 80 min under these conditions. Fourier transform infrared (FTIR) spectra indicated that the MO de-colorization is due to the photocatalytic reaction of photocatalysts rather than adsorption (Figure S11). The CQDs/H-TiO_2 heterostructures exhibited an enhanced degradation rate and degradation efficiency under UV, visible, and NIR light irradiation (Figure 5a–c).

As shown in Figure 5a, the photodegradation efficiency of MO over CQDs/H-TiO_2 heterostructures is more than 86% within 25 min under UV light irradiation. The photocatalytic activity of CQDs/H-TiO_2 heterostructures is superior to P25 (66%), TiO_2 nanobelts (63%), and H-TiO_2 nanobelts (82%). In addition, the UV photocatalytic activity of H-TiO_2 nanobelts is better than that of P25 and TiO_2 nanobelts as well. This can be attributed to the oxygen vacancies and Ti^{3+} created by hydrogenation. The role of Ti^{3+} species can serve as hole scavengers. Also, oxygen vacancies on the surface of TiO_2 nanobelt would act as O_2 binding sites and electron scavengers, thus suppressing the electron-hole recombination and remarkably improve the photocatalytic activity of TiO_2 nanobelt [47]. Under visible light irradiation for 25 min (Figure 5b), CQDs/H-TiO_2 heterostructures (50%) and H-TiO_2 nanobelts (45%) exhibit higher photocatalytic activities than P25 (26%) and pure TiO_2 nanobelts (17%). Among them, CQDs/H-TiO_2 heterostructures exhibited the highest photocatalytic activity under visible light irradiation. Fast electron transfer between CQDs and H-TiO_2 nanobelts can effectively promote the efficient separation of electron-hole (e^--h^+) pairs, thus the visible photocatalytic activities of CQDs/H-TiO_2 heterostructures are enhanced. In addition, the visible photocatalytic activity of H-TiO_2 nanobelts is better than that of P25 and TiO_2 nanobelts as well. This is because H-TiO_2 nanobelts have a narrow band gap and exhibit enhanced visible light absorption in the region of 400–800 nm. It is evident from the results that the H-TiO_2 nanobelts can absorb more visible light than pure TiO_2 nanobelts and thus display better visible photocatalytic activity. Under NIR light irradiation (Figure 5c), we can see that the photodegradation process over CQDs/H-TiO_2 heterostructures is efficient with about 32% MO decomposed after 120 min. In control experiments using P25, TiO_2 nanobelts, and H-TiO_2 nanobelts as photocatalysts, no or little degradation of MO was observed. The TiO_2 nanobelts and H-TiO_2 nanobelts photocatalysts do not respond to light over 740 nm. After CQDs assemble onto the H-TiO_2 nanobelts, the CQDs/H-TiO_2 heterostructures can respond to NIR light. The above experimental results demonstrate that CQDs can play key roles for the enhanced NIR photocatalytic activity. Only light with wavelengths shorter than 530 nm can be used to excite H-TiO_2 nanobelts (bandgap about 2.4 eV) to form photogenerated electron/hole pairs, so the up-converted PL behavior of CQDs may make CQDs/H-TiO_2 heterostructures useful in the NIR light region [48]. The NIR light is harvested by CQDs, converted to visible light, and subsequently excite H-TiO_2 to complete the NIR-photocatalysis process of the hybrid nanobelts.

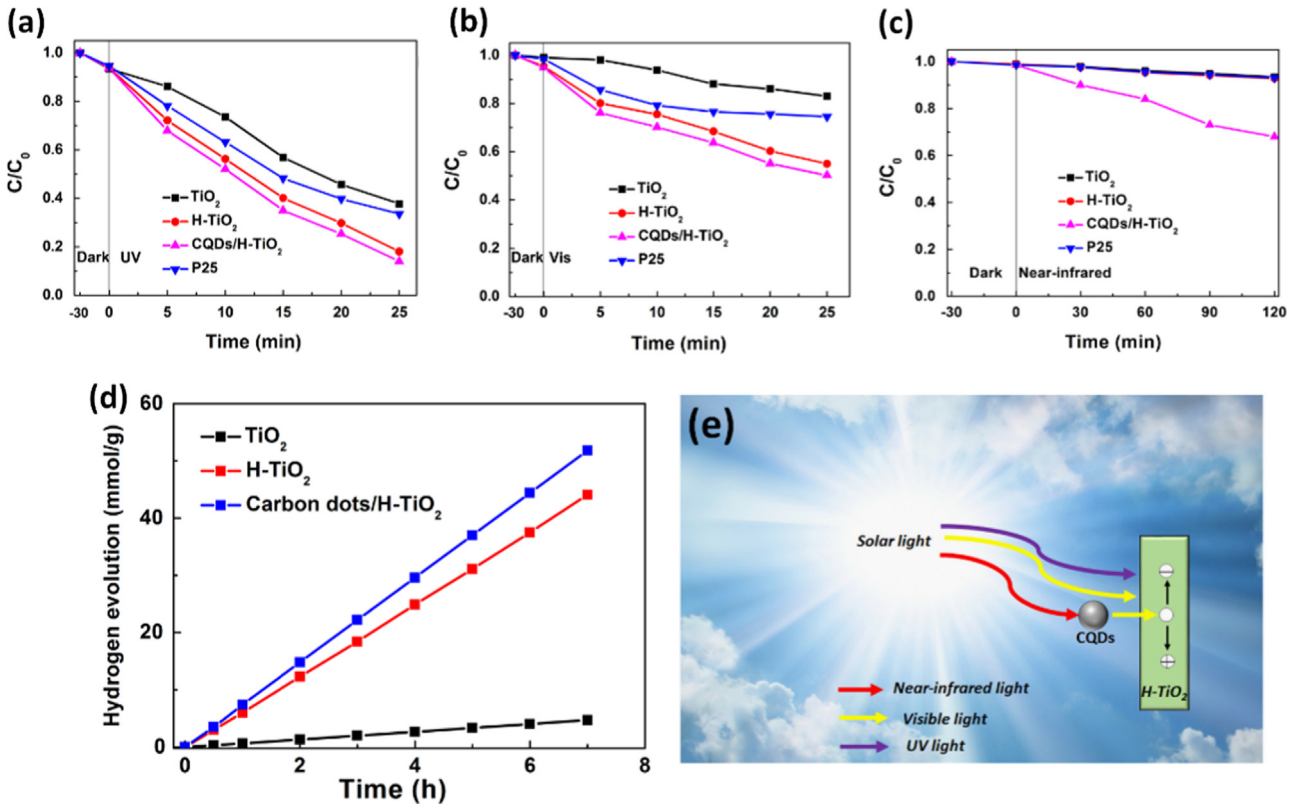

Figure 5 Photocatalytic degradation of MO in the presence of P25, TiO_2 nanobelts, H-TiO_2 nanobelts and CQDs/H-TiO_2 heterostructures under (a) UV, (b) visible, and (c) NIR light irradiation; (d) Photocatalytic hydrogen generation of 1 wt% Pt loaded TiO_2 nanobelts, H-TiO_2 nanobelts, and CQDs/H-TiO_2 heterostructures under Xe arc lamp (300 W); and (e) schematic photocatalytic mechanism for the CQDs/H-TiO_2 heterostructures under UV, visible and NIR light irradiation.

The experiment on photocatalysis cyclic performance of CQDs/H-TiO_2 heterostructures under UV, visible, and NIR light irradiation demonstrates that the samples exhibit the stable performance, i.e. there is no obvious decrease in photocatalytic degradation activity even after four cycles (Figure S12). Then it can be concluded that the CQDs/H-TiO_2 heterostructures really and truly realizes the efficient usage of the full spectrum of sunlight.

To further demonstrate the enhanced photocatalytic property of the CQDs/H-TiO_2 heterostructures, hydrogen evolution was measured for the photocatalytic water-splitting process (Figure 5d). The TiO_2 nanobelts show poor photocatalytic oxygen production activity (0.65 mmol h^{-1} g^{-1}), because they can only absorb UV light. However, the CQDs/H-TiO_2 heterostructures exhibit the highest hydrogen evolution rate of about 7.42 mmol $h^{-1}g^{-1}$, which is higher than that of H-TiO_2 nanobelts (6.01 mmol $h^{-1}g^{-1}$). The obvious photocatalytic oxygen production activities can be attributed to the efficient visible light absorption of H-TiO_2 nanobelts [49]. Importantly, the synergistic effect from the CQDs and the heterostructure's formation makes the photocatalytic hydrogen production activity of CQDs/H-TiO_2 heterostructures higher than that of the pure H-TiO_2 nanobelts. Therefore, in the CQDs/H-TiO_2 heterostructures, the H-TiO_2 nanobelt is expected to act as an efficient light harvester and the heterostructure provides the efficient charge separation to suppress the electron-hole recombination, which greatly enhances the photocatalytic activity in the hydrogen production.

On the basis of the above experimental results, the photocatalytic process of the CQDs/H-TiO_2 heterostructures under UV, visible and NIR light irradiation can be described as schematically illustrated in Figure 5e. (1) When CQDs are attached to the H-TiO_2 nanobelts, the CQDs/H-TiO_2 heterostructures are formed. The heterostructure can enhance the photocatalytic activities by promoting the separation of photo-generated holes and electrons. (2) CQDs/H-TiO_2 heterostructures have a large specific surface area. The Brunauer–Emmett–Teller (BET) surface area of the CQDs/H-TiO_2 heterostructures is estimated to be about 32.91 m^2 g^{-1}, which is higher than that of pure TiO_2 nanobelts (19.01 m^2 g^{-1}) and H-TiO_2 nanobelts (20.01 m^2 g^{-1}). The CQDs/H-TiO_2 heterostructures have a more coarsen surface and larger surface area, which make the CQDs/H-TiO_2 heterostructures absorb more pollutant molecules. Photo-induced electrons and holes can directly degrade these pollutant molecules, thus the photocatalytic properties are improved. (3) CQDs can absorb NIR light (>700 nm), and then emit shorter wavelength light (390–564 nm) as a result of up-conversion, which subsequently excites H-TiO_2 nanobelt to form electron/hole (e^-/h^+) pairs. So the up-converted PL behavior of CQDs make the CQDs/H-TiO_2 heterostructures have the NIR photocatalytic activities.

Conclusions

In summary, a new hybrid photocatalyst (CQDs/H-TiO_2 heterostructures) was synthesized via a simple and efficient

hydrothermal and bath reflux strategy. A layer of dense CQDs are assembled on the surface of H-TiO_2 nanobelts. Importantly, the heterostructures exhibit excellent photocatalytic decomposition of organic dyes activity under wide spectrum (UV, visible, and NIR light) irradiation. The novel photocatalysts further confirm that the oxygen vacancies and Ti^{3+} ions created by hydrogenation and CQDs play key roles in improving the activity of the TiO_2 nanobelts photocatalysts. Oxygen vacancies on the surface of TiO_2 nanobelts, associating with Ti^{3+} sites, can enhance UV and visible light photocatalytic activity through improved optical absorption, charge carrier trapping, and prevention of electron-hole recombination. Meanwhile, the up-converted PL property of CQDs enable the CQDs/H-TiO_2 heterostructures to make use of NIR light by absorption of the visible light converted by CQDs from the NIR light region. Moreover, CQDs with excellent photo-induced electron transfer and reservoir properties can effectively suppress the recombination of electron-hole pairs, thereby leading to significantly enhanced photoelectric conversion efficiency. All of the above allow the heterostructures to have enhanced UV, visible, and NIR light photocatalytic activity. The findings of this work provide further insights into the development of TiO_2 materials as photocatalysts for water splitting under broad spectrum (UV, visible, and NIR light) radiation as well as for other solar energy conversion applications.

Acknowledgments

The authors are thankful to Prof. Nicholas Kotov in University of Michigan, USA for his helpful discussion and very carefully revision on the manuscript, and thankful the funding from the National Natural Science Foundation of China (Grant no. 51372142), National Science Fund for Distinguished Young Scholars (NSFDYS: 50925205), Innovation Research Group (IRG: 51321091). Thanks for the support from "100 Talents Program" of the Chinese Academy of Sciences and the "thousands talents program" for pioneer researcher and his innovation team, China.

Appendix A. Supporting information

Supplementary data associated with this article can be found in the online version at http://dx.doi.org/10.1016/j.nanoen.2014.10.025.

References

[1] J. Qi, K. Zhao, G. Li, Y. Gao, H. Zhao, R. Yu, Z. Tang, Nanoscale 6 (2014) 4072–4077.
[2] Q. Zhang, E. Uchaker, S.L. Candelaria, G. Cao, Chem. Soc. Rev. 42 (2013) 3127–3171.
[3] N.Q. Wu, J. Wang, D. Tafen, H. Wang., J.-G. Zheng, J.P. Lewis, X. Liu, S.S. Leonard, A. Manivannan, J. Am. Chem. Soc. 132 (2010) 6679–6685.
[4] J. Tian, Y. Sang, G. Yu, H. Jiang, X. Mu, H. Liu, Adv. Mater. 25 (2013) 5075–5080.
[5] J.-L. Lan, Z. Liang, Y.-H. Yang, F.S. Ohuchi, S.A. Jenekhe, G. Cao, Nano Energy 4 (2014) 140–149.
[6] L. Wang, T. Sasaki, Chem. Rev. 114 (2014) 9455–9486.
[7] X. Wu, S. Yin, Q. Dong, B. Liu, Y. Wang, T. Sekino, S.W. Lee, T. Sato, Sci. Rep. 3 (2013).
[8] X. Guo, W. Di, C. Chen, X. Wang, W. Qin, Dalton Trans. 43 (2014) 1048–1054.
[9] S.U. Khan, M. Al-Shahry, W.B. Ingler, Science 297 (2002) 2243–2245.
[10] J. Tian, Z. Zhao, A. Kumar, R.I. Boughton, H. Liu, Chem. Soc. Rev. 43 (2014) 6920–6937.
[11] B. Seger, J. McCray, A. Mukherji, X. Zong, Z. Xing, L. Wang, Angew. Chem. Int. Ed. 52 (2013) 6400–6403.
[12] X. Wang, Z. Li, J. Shi, Y. Yu, Chem. Rev. 114 (2014) 9346–9384.
[13] O. Carp, C. Huisman, A. Reller, Prog. Solid State Chem. 32 (2004) 33–177.
[14] J. Tian, Y. Sang, Z. Zhao, W. Zhou, D. Wang, X. Kang, H. Liu, J. Wang, S. Chen, H. Cai, Small 9 (2013) 3864–3872.
[15] J. Lin, J. Shen, R. Wang, J. Cui, W. Zhou, P. Hu, D. Liu, H. Liu, J. Wang, R.I. Boughton, J. Mater. Chem. 21 (2011) 5106–5113.
[16] G. Li, X. Liu, J. An, H. Yang, S. Zhang, P.-K. Wong, T. An, H. Zhao, Catal. Today (2014). http://dx.doi.org/10.1016/j.cattod.2014.05.040.
[17] R. Asahi, T. Morikawa, T. Ohwaki, K. Aoki, Y. Taga, Science 293 (2001) 269–271.
[18] Z. Bian, J. Zhu, S. Wang, Y. Cao, X. Qian, H. Li, J. Phys. Chem. C 112 (2008) 6258–6262.
[19] J. Wang, P. Zhang, X. Li, J. Zhu, H. Li, Appl. Catal. B: Environ. 134 (2013) 198–204.
[20] D.-X. Xu, Z.-W. Lian, M.-L. Fu, B. Yuan, J.-W. Shi, H.-J. Cui, Appl. Catal. B: Environ. 142 (2013) 377–386.
[21] G. Wang, B. Huang, X. Ma, Z. Wang, X. Qin, X. Zhang, Y. Dai, M.H. Whangbo, Angew. Chem. Int. Ed. 125 (2013) 4910–4913.
[22] H. Li, R. Liu, S. Lian, Y. Liu, H. Huang, Z. Kang, Nanoscale 5 (2013) 3289–3297.
[23] L.T. Su, S.K. Karuturi, J. Luo, L. Liu, X. Liu, J. Guo, T.C. Sum, R. Deng, H.J. Fan, X. Liu, Adv. Mater. 25 (2013) 1603–1607.
[24] T. Leshuk, R. Parviz, P. Everett, H. Krishnakumar, R.A. Varin, F. Gu, ACS Appl. Mater. Interfaces 5 (2013) 1892–1895.
[25] X. Chen, C. Li, M. Graetzel, R. Kostecki, S.S. Mao, Chem. Soc. Rev. 41 (2012) 7909–7937.
[26] T. Xia, C. Zhang, N.A. Oyler, X. Chen, Adv. Mater. 25 (2013) 6905–6910.
[27] X. Pan, M.-Q. Yang, X. Fu, N. Zhang, Y.-J. Xu, Nanoscale 5 (2013) 3601–3614.
[28] M. Setvín, U. Aschauer, P. Scheiber, Y.-F. Li, W. Hou, M. Schmid, A. Selloni, U. Diebold, Science 341 (2013) 988–991.
[29] S. Li, J. Qiu, M. Ling, F. Peng, B. Wood, S. Zhang, A.C.S. Appl., Mater. Interfaces 5 (2013) 11129–11135.
[30] H. Li, X. He, Z. Kang, H. Huang, Y. Liu, J. Liu, S. Lian, C.H.A. Tsang, X. Yang, S.T. Lee, Angew. Chem. Int. Ed. 49 (2010) 4430–4434.
[31] H. Zhang, H. Huang, H. Ming, H. Li, L. Zhang, Y. Liu, Z. Kang, J. Mater. Chem. 22 (2012) 10501–10506.
[32] H. Li, R. Liu, Y. Liu, H. Huang, H. Yu, H. Ming, S. Lian, S.-T. Lee, Z. Kang, J. Mater. Chem. 22 (2012) 17470–17475.
[33] X. Zhang, H. Huang, J. Liu, Y. Liu, Z. Kang, J. Mater. Chem. A 1 (2013) 11529–11533.
[34] X. Chen, L. Liu, Y.Y. Peter, S.S. Mao, Science 331 (2011) 746–750.
[35] D. Tang, H. Zhang, H. Huang, R. Liu, Y. Han, Y. Liu, C. Tong, Z. Kang, Dalton Trans. 42 (2013) 6285–6289.
[36] Z. Zhao, J. Tian, D. Wang, X. Kang, Y. Sang, H. Liu, J. Wang, S. Chen, R.I. Boughton, H. Jiang, J. Mater. Chem. 22 (2012) 23395–23403.
[37] H. Li, X. He, Y. Liu, H. Huang, S. Lian, S.-T. Lee, Z. Kang, Carbon 49 (2011) 605–609.
[38] L. Bao, Z.L. Zhang, Z.Q. Tian, L. Zhang, C. Liu, Y. Lin, B. Qi, D.W. Pang, Adv. Mater. 23 (2011) 5801–5806.
[39] Y. Dong, H. Pang, H.B. Yang, C. Guo, J. Shao, Y. Chi, C.M. Li, T. Yu, Angew. Chem. Int. Ed. 52 (2013) 7800–7804.
[40] W. Wei, N. Yaru, L. Chunhua, X. Zhongzi, RSC Adv. 2 (2012) 8286–8288.

[41] X. Lu, G. Wang, T. Zhai, M. Yu, J. Gan, Y. Tong, Y. Li, Nano Lett. 12 (2012) 1690–1696.
[42] S.-T. Myung, M. Kikuchi, C.S. Yoon, H. Yashiro, S.-J. Kim, Y.-K. Sun, B. Scrosati, Energy Environ. Sci. 6 (2013) 2609–2614.
[43] S.H. Szczepankiewicz, J.A. Moss, M.R. Hoffmann, J. Phys. Chem. B 106 (2002) 2922–2927.
[44] M. Wang, L. Sun, Z. Lin, J. Cai, K. Xie, C. Lin, Energy Environ. Sci. 6 (2013) 1211–1220.
[45] Y.-Q. Zhang, D.-K. Ma, Y.-G. Zhang, W. Chen, S.-M. Huang, Nano Energy 2 (2013) 545–552.
[46] T.L. Thompson, J.T. Yates, Chem. Rev. 106 (2006) 4428–4453.
[47] T.L. Thompson, J.T. Yates, Top. Catal. 35 (2005) 197–210.
[48] G. Wang, X. He, G. Xu, L. Chen, Y. Zhu, X. Zhang, L. Wang, Biosens. Bioelectron. 43 (2013) 125–130.
[49] Y.H. Hu, Angew. Chem. Int. Ed. 51 (2012) 12410–12412.

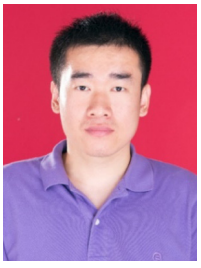

Jian Tian obtained his B.Sc. degree from Beijing University of Chemical Technology in 2008. Currently, he is pursuing his Ph.D. degree under the supervision of Prof. Hong Liu in State Key Laboratory of Crystal Materials, Shandong University, China. His research interest in his Ph.D. study is mainly focused on preparation and modifications of one-dimensional TiO_2 nanostructured surface heterostructures for photocatalysis applications.

Yanhua Leng obtained his B.Sc. degree from Shandong University in 2012. Currently, he is pursuing his M.Sc. degree under the supervision of Prof. Hong Liu in State Key Laboratory of Crystal Materials, Shandong University, China. His research is mainly focused on the first-principle calculation and crystal growth simulation.

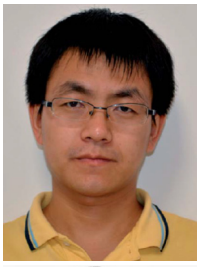

Zhenhuan Zhao received his M.Sc. degree from Shandong Polytechnic University in 2011. Currently he is pursuing his Ph.D. degree under the supervision of Prof. Hong Liu at the State Key Laboratory of Crystal Materials in Shandong University, China. His research is mainly focused on nanomaterials for sustainable energy and energy storage based on supercapacitors.

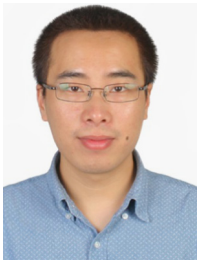

Dr. Yang Xia received his Ph.D. degree in June 2013 at Zhejiang University of Technology with Prof. Wenkui Zhang. Now, he works as a lecturer in College of Materials Science and Engineering, Zhejiang University of Technology, China. He mainly works on the development of nanostructured carbon based materials for energy storage and conversion, including lithium ion batteries, lithium-sulfur and supercapacitors.

Dr. Yuanhua Sang obtained his B.S. degree at Shandong University in China in 2007 and completed his Ph.D. with Prof. Hong Liu at Shandong University in July 2012. Now, he works as a lecturer in State Key Laboratory of Crystal Materials, Shandong University, China. His research interests are structure and property investigation of inorganic crystal materials with neutron and x-ray diffraction, functional materials, and materials for solar light conversion.

Pin Hao is pursuing his Ph.D. under the supervision of Prof. Hong Liu at the State Key Laboratory of Crystal Materials in Shandong University, China. Her research interests lie in the fields of supercapacitor and photocatalystor, nano-functional material syntheses and characterizations, hierarchical porous carbon and graphene aerogels using biopolymers.

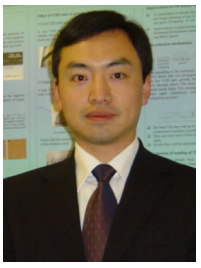

Dr. Meicheng Li is professor in State Key Laboratory of Alternate Electrical Power System with Renewable Energy Sources, North China Electric Power University. He received his PhD degree in 2001 from Harbin Institute of Technology. Dr. Li's current main focus is silicon nanowire based photovoltaic devices, including fundamental understanding, applied research and development (R&D), and flexible device design. He also has interest in R&D of perovskite solar cells, lithium ion battery system and other renewable energy.

Dr. Hong Liu is professor in State Key Laboratory of Crystal Materials, Shandong University, and adjunct professor in Beijing Institute of Nanoenergy and Nanosystem, Chinese Academy of Science. He received his Ph.D. degree in 2001 from Shandong University (China). His current research is focused mainly on nonlinear crystal growth, chemical processing of nanomaterials for energy related applications including photocatalysis, tissue engineering, especially the interaction between stem cell and nanostrucuture of biomaterials.